Strategies for developing flavonoids with multiple reactivities against pathological features in Alzheimer's disease

Seongmin Park,[‡a] Mingeun Kim,[‡a] Yuxi Lin,[b] Mannkyu Hong,[ac] Geewoo Nam,[a] Adam Mieczkowski,[d] Young-Ho Lee*[befg] and Mi Hee Lim*[a]

[a]Department of Chemistry, Korea Advanced Institute of Science and Technology (KAIST), Daejeon 34141, Republic of Korea

[b]Research Center for Bioconvergence Analysis, Korea Basic Science Institute (KBSI), Ochang, Chungbuk 28119, Republic of Korea

[c]Center for Catalytic Hydrocarbon Functionalizations, Institute for Basic Science (IBS), Daejeon 34141, Republic of Korea

[d]Institute of Biochemistry and Biophysics, Polish Academy of Sciences, Pawińskiego 5a, 02-106 Warsaw, Poland

[e]Neurovascular Research Group, Korea Brain Research Institute (KBRI), Daegu 41068, Republic of Korea

[f]Bio-Analytical Science, University of Science and Technology (UST), Daejeon 34113, Republic of Korea

[g]Graduate School of Analytical Science and Technology, Chungnam National University, Daejeon 34134, Republic of Korea

[‡]These authors contributed equally to this work.

*To whom correspondence should be addressed: miheelim@kaist.ac.kr and mr0505@kbsi.re.kr

Abstract

The etiology of Alzheimer's disease (AD) is still unknown because of its complicated nature associated with various pathological components, including free radicals, acetylcholinesterase, and metal-free and metal-bound amyloid-β. Thus, chemical reagents with modulating reactivities against multiple pathogenic factors are necessary for advancing our understanding of the complex pathogenesis. Here we report rational strategies for developing flavonoids that can control multiple pathological elements found in the brains of AD patients. Our investigations employing a series of flavonoids illuminated structural features critical for regulatory reactivities against desired targets. Moreover, the most promising flavonoid with multiple functions was developed based on our complete structure–activity relationship. Mechanistic studies confirmed that such versatile reactivities of the flavonoid are achieved by its redox potential and direct interactions with pathogenic factors. Overall, our studies demonstrate the feasibility of devising small molecules as multifunctional chemical reagents against pathological features found in AD.

Introduction

The intertwined network among multiple pathological factors, such as free radicals, acetylcholinesterase (AChE), metal-free amyloid-β (Aβ), and metal-bound Aβ (metal–Aβ) (Fig. 1a and b), has given the difficulty in combating Alzheimer's disease (AD).[1–5] Oxidative stress characterized by dysregulated free radicals can damage lipids, nucleic acids, and proteins, which leads to organelle dysfunction and apoptosis.[6–8] As illustrated in the cholinergic hypothesis, AChE is associated with the development of AD.[3,9] The synaptic concentration of the neurotransmitter acetylcholine (ACh) is adjusted by the catalytic activity of AChE;[10–12] however, the abnormally reduced level of ACh can be driven by the increased amount of AChE.[3,10,13] In addition, highly concentrated AChE within senile plaques (SPs) can colocalize and interact with Aβ species, resulting in the AChE–Aβ complexation and the acceleration of amyloid aggregation.[13,14] Aβ peptides tend to aggregate into oligomers and fibrils.[15,16] In particular, metastable and structured Aβ oligomers are known to cause toxicity in cellular systems by triggering membrane disruptions, abnormal cellular signaling, and organelle dysfunction.[1,9,15] High concentrations of metal ions [*e.g.*, Cu(I/II) and Zn(II)] are also found in the SPs of AD patients, and they can affect the conformation and aggregation behaviors of Aβ by their coordination to Aβ.[17,18] Moreover, redox-active Cu(I/II)-bound Aβ species can produce reactive oxygen species *via* Fenton-like reactions and, consequently, aggravate oxidative stress.[19–21]

Several pharmacological trials employing antioxidants (*e.g.*, vitamin E),[22,23] AChE inhibitors (*e.g.*, donepezil, galantamine, rivastigmine),[3,19] and anti-Aβ drugs (*e.g.*, aducanumab)[24,25] have been attempted to prevent the progression of AD. Such single target-based therapeutics can temporarily relieve symptoms,[3,19] and their efficacies are still questionable, however.[9,26] Thus, significant endeavors in designing chemical reagents capable of targeting and modulating two or more pathogenic elements have been made to elucidate the complex pathology of AD and discover effective therapeutic candidates.[3,9] Herein, we illustrate rational approaches for developing flavonoids that can target multiple pathogenic factors, including free radicals, AChE, metal-free Aβ, and metal–Aβ, as depicted in Fig. 1a, and modulate their reactivities. We identified key structural features shown in flavonoids that are responsible for versatile reactivities against desired pathological targets through structure–activity relationship studies. Moreover, the most promising flavonoid with multiple functions was developed based on our structure–activity relationship analyses, with the determination of molecular-level mechanistic details. Our overall work demonstrates the development of flavonoids as small molecule-based chemical reagents capable of controlling multiple pathological components associated with neurodegenerative

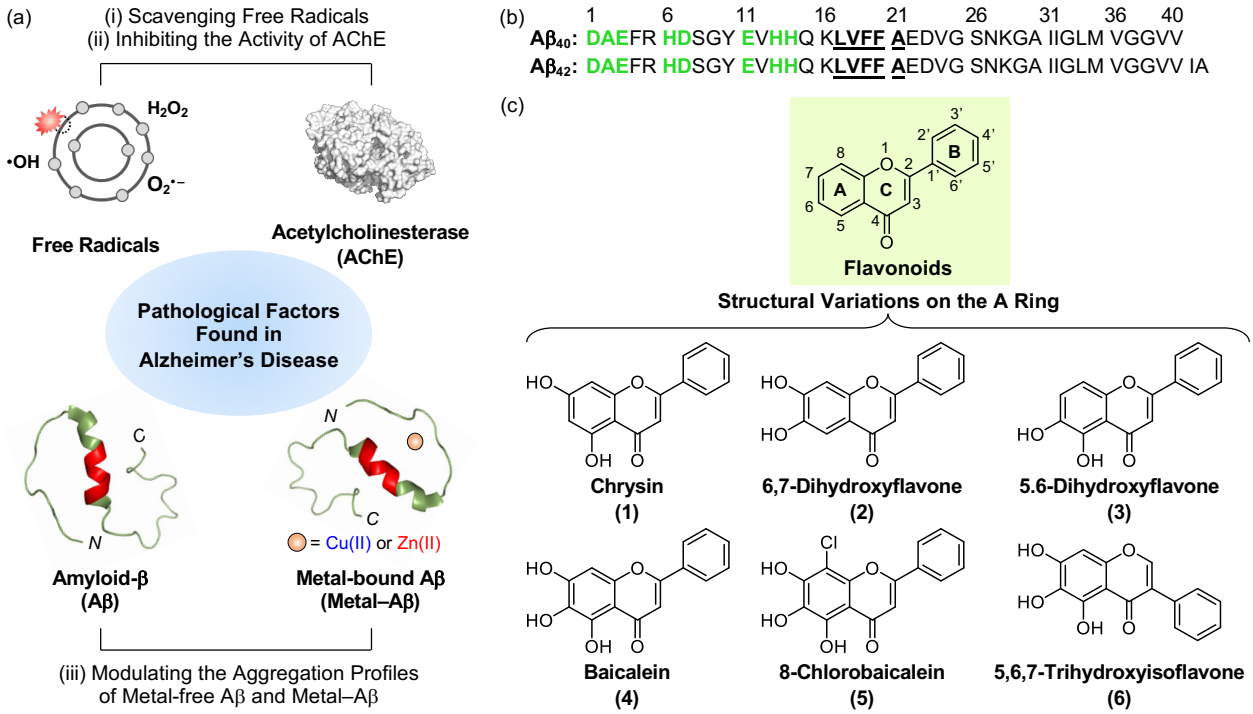

Fig. 1 Multiple pathogenic factors and flavonoids investigated in this work. (a) Free radicals, AChE (PDB 1C2B[50]), metal-free Aβ (PDB 2LFM[16]), and metal–Aβ as pathological elements to be controlled in this work. (b) Sequences of Aβ peptides. Amino acid residues involved in the metal-binding and self-recognition sites are highlighted in bold (green and underline, respectively). (c) Chemical structures of the flavonoids (**1**–**6**).

disorders, such as AD.

Results and discussion

Selection and preparation of 1–6

Given that flavonoids as a family of naturally occurring polyphenols have antioxidant,[27] antiviral,[28] anticancer,[29] and antimicrobial activities,[30] we chose the flavonoid framework for our molecular design of small molecules with reactivities of multiple pathological targets. As presented in Fig. 1c, some structural moieties of flavonoids are reported to be important for modulating free radicals, AChE, metal-free Aβ, and metal–Aβ: (i) The unsaturated bond between C2 and C3 on the C ring of flavonoids could interact with the hydrophobic self-recognition (Leu17–Ala21) and *C*-terminal regions of Aβ that are essential for its aggregation process;[31–34] (ii) the 4-oxo functionality on the

C ring as an oxygen (O) donor atom can participate in metal coordination;[35] (iii) the chromone moiety (A and C rings) is responsible for the reactivity of flavonoids against AChE through the interactions with amino acid residues containing an aromatic ring at their side chains (*e.g.*, Trp86, Phe295, and Tyr341) within the hydrophobic binding pocket of AChE;[36] (iv) both the number and position of hydroxyl groups are associated with redox properties of flavonoids.[37]

In addition to the abovementioned structural features of flavonoids, the incorporation of hydroxyl groups on the B and C rings and the isoflavone variation to regulate pathological factors have been recently identified;[35,36,38] however, the information on structural and chemical properties on the A ring for multiple reactivities towards our desired targets, except for AChE,[39] is very limited. Thus, to gain a full spectrum of the structure–activity relationship with respect to all the A, B, and C rings, we rationally selected a series of six flavonoids (**1**–**6**; Fig. 1c) through the structural variation of hydroxyl groups on the A ring that can alter their electronic and AChE-/Aβ-interacting properties. Compounds **1**–**3** containing two hydroxyl groups located at distinct positions on the A ring were first chosen. Our series also included **4** possessing three hydroxyl groups on the A ring. Compound **5** that embodies three hydroxyl groups with an electron-withdrawing chloro group at the C8 position on the A ring was additionally selected, along with **6** as a regioisomer of **4** with an isoflavone moiety. Compounds **1**–**6** were obtained from commercially available sources (**1**–**4**) or prepared by previously reported synthetic routes (**5**[40] and **6**[41]). The characterization of **5** and **6** was summarized in Figs. S1 and S2, respectively.

Redox potentials and scavenging capability against free organic radicals

The redox activity of small molecules is critical for controlling multiple pathological features of AD, including free radicals, metal-free Aβ, and metal–Aβ.[37,42–45] In particular, redox properties of small molecules are connected with their antioxidant ability.[46] Thus, the redox potentials of **1**–**6** were first computed following the previously reported density-functional theory (DFT) calculation.[47] It should be noted that the electrochemical determination of flavonoids is very challenging due to their instability and limited solubility in aqueous media and organic solvents. As illustrated in Fig. 2a, the calculated redox potentials were varied with the number and position of electron-donating hydroxyl groups on the A ring. Based on the position of hydroxyl groups on the A ring shown in **1**–**3**, their $E°$ values *vs.* standard hydrogen electrode (SHE) were ranged from 1.440–1.534 V. In detail, the incorporation of two hydroxyl substituents *ortho*-positioned at either C6/C7 (**2**) or C5/C6 (**3**) decreased the redox potentials, relative to that at the *meta*-position (C5/C7, **1**). Furthermore, **4** with an additional hydroxyl group on the A ring revealed a lower redox potential, compared to **1**–**3**. Introducing an electron-withdrawing chloro substituent at the C8 position and switching the

(a)

Compound	*E*° (Calc.) (V *vs.* SHE)	TEAC Value
1	1.534	n.d.[a]
2	1.440	1.15 ± 0.06
3	1.477	0.98 ± 0.05
4	1.225	1.61 ± 0.09
5	1.463	1.04 ± 0.02
6	1.202	1.66 ± 0.04
7	1.018	2.30 ± 0.04

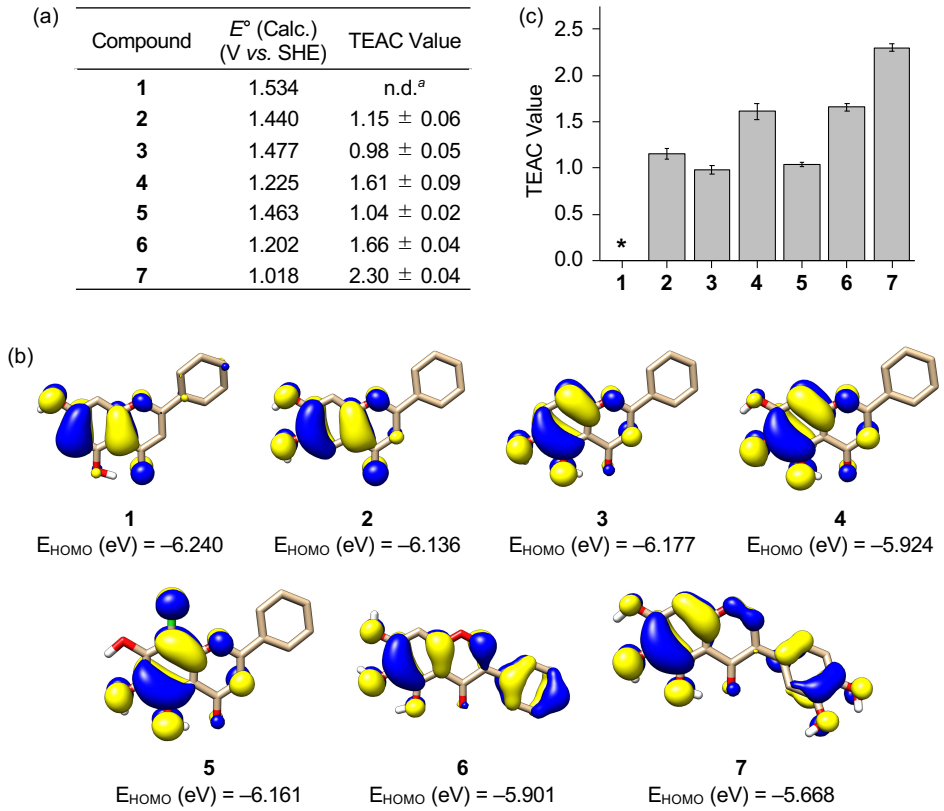

Fig. 2 Redox properties of **1**–**7** and their ability to quench free organic radicals. The (a) redox potentials (*E*° *vs*. SHE) of **1**–**7** were calculated with the (b) isosurface plots (isodensity value = 0.03 a.u.) of their HOMOs. (a and c) TEAC values of **1**–**7** determined by the TEAC assay. Conditions: EtOH; 25 °C; λ_{abs} = 734 nm. [a]n.d., not determined. *Note that the TEAC value of **1** could not be obtained due to its limited solubility in EtOH.

position of the B ring, presented in **5** and **6**, respectively, indicated higher and lower calculated *E*° values, respectively, than its parent structure **4**.

To obtain a greater understanding of computed redox potentials, the highest occupied molecular orbitals (HOMOs) of **1**–**6** were analyzed. As displayed in Fig. 2b, **1** exhibited the lowest HOMO level among **1**–**6**, which is correlated with the calculated *E*° value. The orbital lobes localized at the C5–C7 positions in the HOMOs of **1**–**3** showed that electron-donating groups at those positions may effectively elevate the HOMO level. In good agreement with this expectation, the HOMO level of **4** carrying three hydroxyl groups at all the C5, C6, and C7 positions was reached at –5.924 eV, which became lower (for **5**) when an electron-withdrawing moiety was substituted at the C8 position. The translocation of an electron-rich phenyl ring (B ring) from δ^+-

charged β-carbon (C2) to δ^--charged α-carbon (C3) offered a higher HOMO level of **6** due to the unfavorable π–conjugation on the C ring enone, compared to **4**.

To determine the ability of **1**–**6** to quench free organic radicals, we performed the Trolox equivalent antioxidant capacity (TEAC) assay employing the cationic radical form of 2,2'-azino-bis(3-ethylbenzthiazoline-6-sulphonic acid).[48] As presented in Fig. 2a and c, compounds were tested, except for **1** that has limited solubility in ethanol under our experimental conditions. Compounds **2**–**6** showed the TEAC values close or over 1.0, relative to a vitamin E analog Trolox, suggesting that their radical scavenging ability is similar or greater than that of Trolox. As anticipated from the calculated *E*° values, relatively low TEAC values were observed for **2** and **3** over **4** and **6**. This investigation manifests the significance of the number of hydroxyl groups on the A ring towards redox properties and antioxidant activity. Despite three hydroxyl groups on the A ring, **5** with an electron-withdrawing chloro group displayed a similar TEAC value with **2** and **3** containing two hydroxyl groups. Our computational and experimental studies confirm that the flavonoid (**6**) embodying three hydroxyl groups without an electron-withdrawing substituent on the A ring can has the lowest redox potential among **1**–**6**, with the consequent noticeable radical scavenging ability.

Inhibition against AChE

Inhibiting the activity of AChE can maintain a proper level of ACh under dysregulated cholinergic conditions.[10,11] Thus, the inhibitory capability of **1**–**6** against AChE was investigated by a previously reported fluorescent AChE assay with slight modifications.[49] As summarized in Fig. 3a, the IC_{50} values of **2**–**6** were in a micromolar range (IC_{50} = 1.40–12.34 μM). It should be noted that the IC_{50} value of **1** could not be obtained due to its negligible AChE inhibition under our experimental conditions. As expected, **4** and **6** that contain three hydroxyl groups on the A ring among our molecules exhibited relatively low IC_{50} values. The inclusion of three hydroxyl groups on the A ring is critical for controlling the catalytic activity of AChE, as previously reported,[39] whereas the incorporation of a chloro substituent on the A ring, with three hydroxyl groups, can decline such inhibitory activity. The noticeable AChE inhibition by **2** and **3** over **1** illustrates the importance of the position of hydroxyl moieties on the A ring in directing compounds' activity against AChE.

Docking studies were further conducted to visualize potential interactions between the flavonoids (**1**–**6**) and AChE employing an X-ray crystal structure of *electrophorus electricus* AChE (PDB 1C2B[50]). As displayed in Figs. 3b and S3, the flavonoids can interact with neighboring amino acid residues that lie in the active site of AChE *via* hydrogen bonding. For example, hydroxyl

(a)

Compound	1	2	3	4	5	6	7
IC_{50} (μM)	n.d.[a]	4.18 (± 0.45)	4.51 (± 0.03)	1.95 (± 0.11)	12.34 (± 1.46)	1.40 (± 0.18)	0.19 (± 0.06)

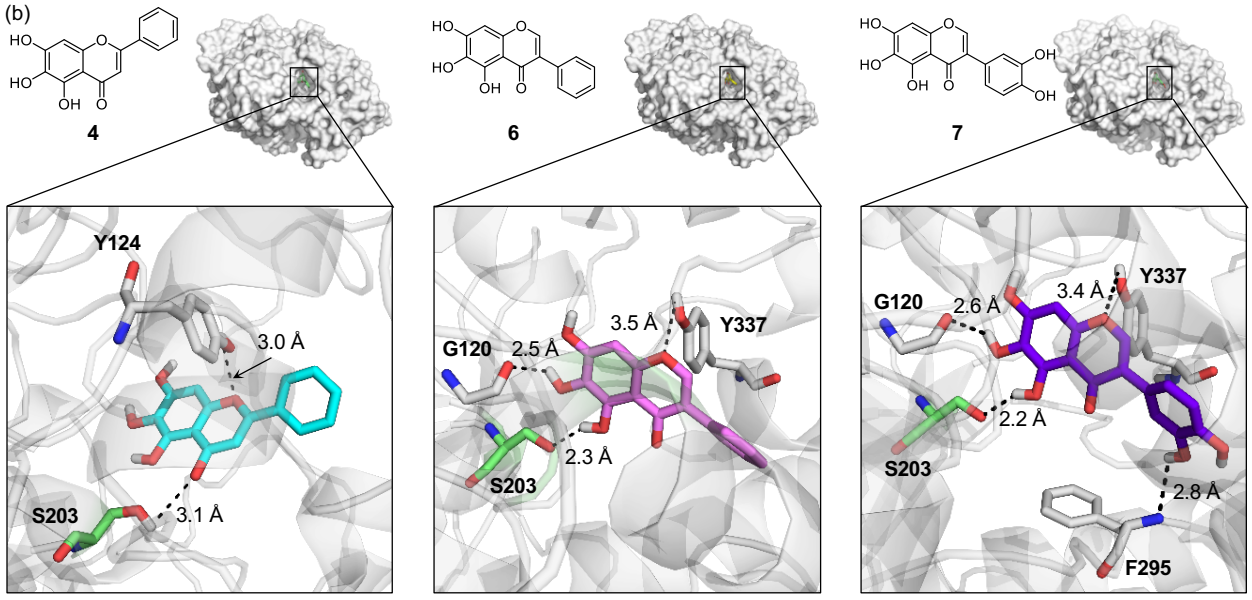

Fig. 3 Inhibitory ability of **1**–**7** against AChE. (a) IC_{50} values of **1**–**7** for AChE inhibition determined by a fluorometric assay. [a]n.d., not determined. Note that the IC_{50} value of **1** could not be obtained due to its low inhibitory activity against AChE. (b) Possible intermolecular interactions of **4**, **6**, and **7** against AChE (PDB 1C2B[50]) visualized by docking studies. Nine docked models of **4**, **6**, and **7** against AChE with binding energies ranging from –10.8 to –8.7 kcal/mol were obtained. The representative models with the highest binding affinity towards AChE are shown in the figure. Hydrogen bonds between compounds and AChE are indicated with dashed lines (2.2−3.5 Å). N, O, H, and C (from Ser203) atoms are depicted in blue, red, white, and green, respectively.

groups on the A ring could serve as a hydrogen-bond donor to interact with the backbone amide group between Gly121 and Gly122 (for **1** and **2**), the backbone carbonyl moiety of Gly120–Gly121 (for **3** and **6**), and the hydroxyl group of Ser203 (for **6**) in AChE. In addition, hydrogen bonds mediated by the central O donor atom and the 4-oxo functionality on the C ring with Tyr337/Tyr341 (for **1** and **2**), Gly122/Tyr124 (for **3**), Tyr124/Ser203 (for **4**), Tyr124 (for **5**), and Tyr337 (for **6**) were also monitored. Anchoring the flavonoids into the active site gorge of AChE could prevent the substrate binding and, ultimately, inhibit the activity of AChE. In particular, hydrogen bonds between Ser203 at the catalytic triad and the 4-oxo functionality on the C ring of **4** or the hydroxyl

group on the A ring of **6** were indicated within 3.1 Å and 2.3 Å, respectively. The Ser203 residue is responsible for initiating the hydrolysis of ACh through hydrogen bonding;[51] thus, the intermolecular interaction with Ser203 could dominantly restrict ACh from binding into the active site of AChE. Overall, these observations highlight the pertinent role of some structural features, such as hydroxyl groups on the A ring and the C ring that contains two O donor atoms, in controlling the catalytic activity of AChE. It should be noted that the π–π stacking between the flavonoids' chromone moiety (A and C rings) and amino acid residues at the anionic subsite of AChE could afford the stability for their positioning at the active site gorge of AChE,[36] but our docking studies were not able to visualize such π–π stacking interactions.

Effects on Aβ aggregation in the absence and presence of metal ions

To verify whether **1**–**6** can modulate the aggregation of Aβ with and without metal ions, the molecular weight (MW) distribution and morphology of the resultant Aβ species were determined by gel electrophoresis with Western blotting (gel/Western blot) using an anti-Aβ antibody (6E10) and transmission electron microscopy (TEM), respectively. Two types of experiments were carried out employing two major Aβ isoforms, *i.e.*, $A\beta_{42}$ and $A\beta_{40}$:[19] (i) Inhibition studies (Fig. 4a) to identify the effect of **1**–**6** on the formation of Aβ aggregates; (ii) disaggregation studies (Fig. S4a) to evaluate if the flavonoids can disassemble preformed Aβ aggregates or modulate their further aggregation.

As presented in Figs. 4b and S5a, the inhibition experiments with metal-free $A\beta_{42}$ showed the notably varied MW distribution upon treatment of **4**–**6**, compared to **1**–**3**. Compounds **4**–**6** discernably reduced the signal intensity of the bands corresponding to $A\beta_{42}$ with the MWs from *ca.* 4–20 kDa and larger than *ca.* 100 kDa, while **1**–**3** may not be able to change the size distribution of metal-free $A\beta_{42}$ species. In the case of Cu(II)–$A\beta_{42}$ incubated with **3** over compound-untreated Cu(II)–$A\beta_{42}$ or Cu(II)–$A\beta_{42}$ treated with **1** and **2**, more intense smearing was monitored in the MW window larger than *ca.* 25 kDa. The sample of Cu(II)–$A\beta_{42}$ incubated with **4** displayed the enhanced level of dodecameric or larger $A\beta_{42}$ aggregates (*ca.* ≥ 50 kDa), with the decreased intensity of the bands assigned to monomeric, dimeric, trimeric, and tetrameric $A\beta_{42}$. The alteration of the size distribution of Cu(II)–$A\beta_{42}$ induced by **5** and **6** was similar to that by the addition of **3**. Comparable to Cu(II)–$A\beta_{42}$, the size distribution of Zn(II)–$A\beta_{42}$ species was modified by **4**–**6**, with the indication of smearing bands at *ca.* 25–240 kDa, while **3** gave rise to increased signal intensity between *ca*. 25–75 kDa. In contrast, a remarkable change in the MW distribution was not indicated by addition of **1** and **2**.

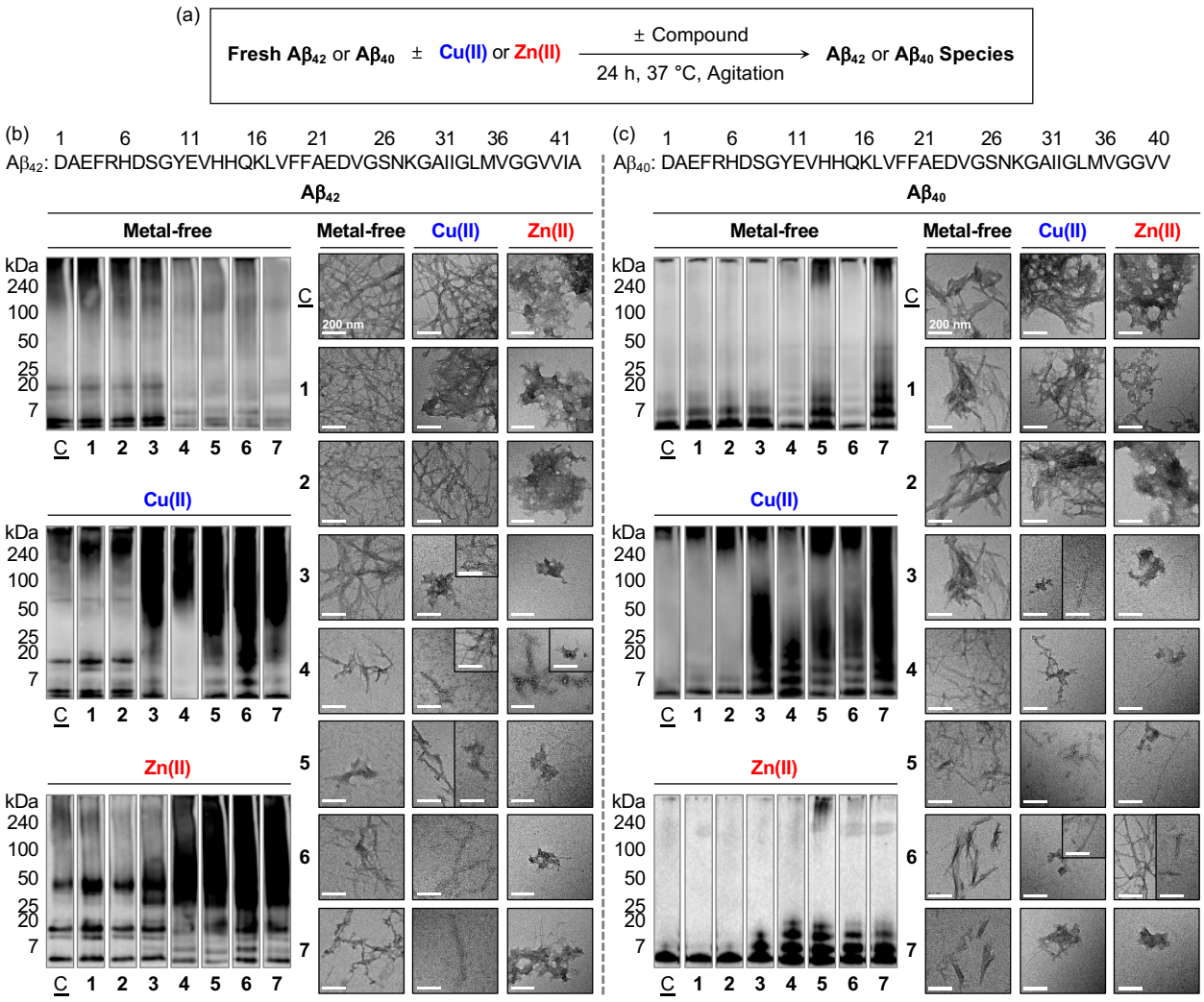

Fig. 4 Effects of **1**–**7** on the formation of metal-free Aβ and metal–Aβ aggregates. (a) Scheme of the inhibition experiments. MW distributions and morphologies of the resultant (b) $A\beta_{42}$ and (c) $A\beta_{40}$ species were analyzed by gel/Western blot with an anti-Aβ antibody (6E10) and TEM, respectively. Lanes: (C) Aβ ± Cu(II) or Zn(II); (**1**) C + **1**; (**2**) C + **2**; (**3**) C + **3**; (**4**) C + **4**; (**5**) C + **5**; (**6**) C + **6**; (**7**) C + **7**. The original gel images are shown in Fig. S5a.† Conditions: [Aβ] = 25 μM; [M(II)] = 25 μM; [compound] = 50 μM (1% v/v DMSO); 20 mM HEPES, pH 7.4, 150 mM NaCl; 37 °C; 24 h; constant agitation. Scale bars = 200 nm.

TEM investigations further supported the flavonoids' reactivity towards the aggregation of $A\beta_{42}$. As illustrated in Fig. 4b, the resultant metal-free $A\beta_{42}$ aggregates produced with **4**–**6** exhibited noticeably different morphologies from compound-untreated $A\beta_{42}$ aggregates, while little

or no morphological alteration was observed from those incubated with **1**–**3**. Metal-free Aβ_{42} added with **4** generated shorter and thinner fibrils with a decrease in their branching. When **5** and **6** were treated with metal-free Aβ_{42} species, smaller fibrils and less structured aggregates were monitored than those obtained from compound-unadded metal-free Aβ_{42}. In the case of Cu(II)–Aβ_{42}, **3**–**6** could vary the morphology of the resultant aggregates. A mixture of amorphous and small fibrillary aggregates was detected upon incubation of **3** and **5** with Cu(II)–Aβ_{42}, relative to a bunch of fibrils observed upon incubation of Cu(II)–Aβ_{42} only. The samples of Cu(II)–Aβ_{42} with **4** and **6** showed chopped and thin fibrils. The resultant aggregates of Zn(II)–Aβ_{42} were notably different by treatment of **3**–**6**, compared to large amorphous species observed in the sample of Zn(II)–Aβ_{42} only. Compounds **3** and **6** triggered the formation of small amorphous aggregates. The addition of **4** to Zn(II)–Aβ_{42} led to the generation of chopped fibrils. In the presence of **5**, both amorphous and fibrillary Zn(II)–Aβ_{42} aggregates were monitored. As expected from our gel/Western blot analysis, **1** and **2** did not indicate any noticeable morphological modifications of the resultant Cu(II)–Aβ_{42} and Zn(II)–Aβ_{42} aggregates.

The impact of **1**–**6** on the aggregation of metal-free Aβ_{40} and metal–Aβ_{40} was similar to that observed with metal-free and metal-added Aβ_{42}. As illustrated in Figs. 4c and S5a, under metal-free conditions, the signal intensity of the bands from *ca.* 7–20 kDa assigned to smaller oligomeric Aβ_{40} species was reduced by **4** and **6**, while **5** increased the band intensity associated with the species larger than *ca.* 7 kDa. When **3**–**6** were treated to Cu(II)–Aβ_{40} and Zn(II)–Aβ_{40}, the resultant Aβ species indicated the diverse MW distribution in the range of *ca.* 7–240 kDa to different extents. As shown in TEM images, shorter and thinner fibrils were generated in the samples of metal-free Aβ_{40} with **4**–**6**. For Cu(II)–Aβ_{40}, **5** formed chopped filamentous Cu(II)–Aβ_{40} aggregates, and **3**, **4**, and **6** produced both amorphous and fibrillary aggregates. These morphological changes were similar to those of Zn(II)–Aβ_{40} incubated with **3**–**5**, and **6** generated a bunch of fibrillary species with chopped filamentous aggregates. Moreover, the disaggregation experiments exhibited the effects of **1**–**6** on preformed Aβ_{42} and Aβ_{40} aggregates in the absence and presence of Cu(II) and Zn(II), as summarized in Figs. S4b and c and S5b. Compounds **4**–**6** could disassemble preformed metal-free Aβ and metal–Aβ aggregates and modulate their further aggregation. In the case of **3**, the reactivity was only shown in the presence of metal ions. Compounds **1** and **2** showed a less noticeable impact on preformed metal-free and metal-treated Aβ aggregates. Collectively, our gel/Western blot and TEM studies demonstrate that **4**–**6** can modulate the fibrillization of Aβ in the absence and presence of metal ions as well as disassemble preformed metal-free Aβ and

metal–Aβ aggregates. In contrast, among the flavonoids (**1**–**3**) containing two hydroxyl groups on the A ring, **3** exhibits the corresponding reactivities only towards metal-mediated Aβ aggregation pathways. These indications describe the significance of three hydroxyl groups on the A ring in the flavonoid structure to impact the aggregation of metal-free Aβ and metal–Aβ.

Rational selection, redox potential, synthesis, and cytotoxicity of 7

Based on the structure–activity relationship observed employing **1**–**6** (Fig. 1c) with the previously reported studies of flavonoids,[36,38,39] we could determine structural features on all the A, B, and C rings of flavonoids that are critical for controlling multiple pathological factors, *i.e.*, free radicals, AChE, metal-free Aβ, and metal–Aβ. As depicted in Fig. 5, first, three hydroxyl groups at the C5–C7 positions on the A ring are essential for gaining multiple reactivities with our desired pathogenic targets. Second, the translocation of the B ring from C2 to C3 on the C ring affording an isoflavone framework can enhance both antioxidant and AChE inhibitory abilities. Third, a catechol moiety on the B ring in an isoflavone backbone is reported to be important in modulating the reactivities of our targets.[36] Moreover, as illustrated in Fig. 2b, comparing the HOMOs of **4** and **6** indicates that the electronic distribution on all the A, B, and C rings is notable in the isoflavone **6**; thus, the addition of electron-donating groups at the C3' and C4' positions on the B ring can impact the electronic property of the overall structure. Collectively, we rationally fashioned the isoflavone **7** (Fig. 5) that contains three hydroxyl groups on the A ring and a catechol moiety on the B ring, as a flavonoid with multiple reactivities against pathological components in AD. As expected, **7** showed the most negative redox potential among all compounds, as shown in Fig. 2a. The addition of a catechol moiety on the B ring from an isoflavone **6** involving three hydroxyl groups on the A ring lowered the redox potential of the compound from 1.202 to 1.018 V (*vs.* SHE). The orbital lobes localized between C3' and C4' in the HOMO of **7** can rationalize its more elevated HOMO level with the subsequent negative calculated $E°$ value, compared to that of **6**, as displayed in Fig. 2a and b.

Compound **7** was synthesized following previously reported procedures with modifications.[52–54] As presented in Scheme 1 and Figs. S6–S8, the Friedel-Crafts acylation of **7a** with **7b** afforded **7c** in the presence of boron trifluoride ethyl etherate (BF_3OEt_2) as both the catalyst and solvent. Compound **7d** was prepared by the subsequent cyclization reaction of **7c** using methanesulfonyl chloride ($MeSO_2Cl_2$), and the final product **7** was obtained *via* the demethylation reaction of **7d** with boron tribromide (BBr_3). After the preparation, the cytotoxicity of **7**, compared to **1**–**6**, was determined by MTT assay employing human neuroblastoma SH-SY5Y cells [MTT = 3-(4,5-dimethylthiazol-2-yl)-2,5-diphenyltetrazolium bromide]. As summarized

in Fig. S9, greater than *ca.* 90% survival at up to 100 μM was observed upon the cells treated with **7** for 24 h. In contrast, the cells upon incubation with 100 μM of **1**–**6** indicated *ca*. 30%, 60%, 50%, 70%, 60%, and 70% viability, respectively. Thus, **7** over **1**–**6** has relatively low cytotoxicity.

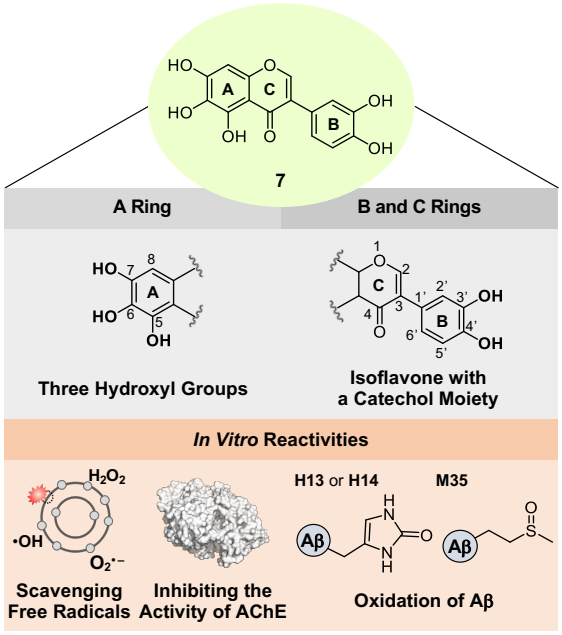

Fig. 5 Design rationale of **7** [3-(3,4-dihydroxyphenyl)-5,6,7-trihydroxy-4*H*-chromen-4-one] and its reactivities against free radicals, AChE, metal-free Aβ, and metal–Aβ.

Scheme 1 Synthetic routes to **7**.

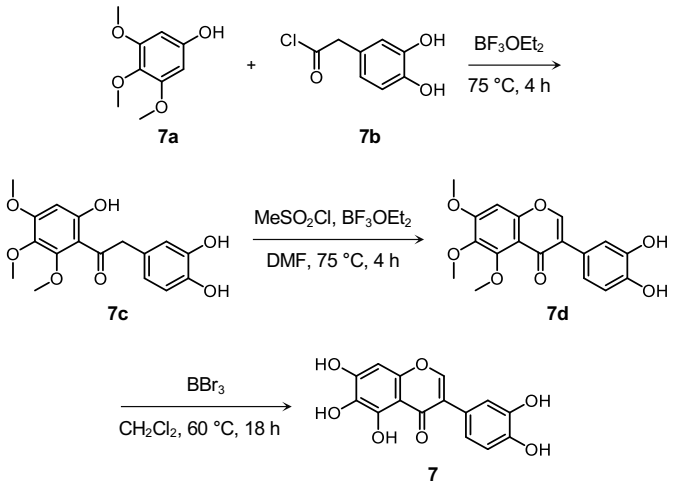

Reactivities of 7 with free organic radicals, AChE, metal-free Aβ, and metal–Aβ

Compound **7** exhibited the significant scavenging capability towards free organic radicals with the highest TEAC value [2.30 (± 0.04)] among our flavonoid series (**1**–**7**), as shown in Fig. 2a and c. In addition, the most remarkable inhibition against the activity of AChE was observed by **7** with a nanomolar IC_{50} value (Fig. 3a). To visualize the potential interactions of **7** with AChE, docking studies were conducted. As illustrated in Fig. 3b, the hydroxyl groups on the A and B rings and the central O donor atom on the C ring could have hydrogen bonds with the backbone carbonyl moiety of Gly120–Gly121, the hydroxyl group of Ser203 and Tyr337, and the backbone amide group between Ile294 and Phe295 within the active site gorge of AChE. Especially, a hydrogen bond between the hydroxyl group at the C5 position on the A ring and Ser203 at the catalytic triad was indicated within 2.2 Å. Moreover, the number of hydrogen bonds between **7** and amino acid residues in the substrate-binding pocket of AChE was increased to four, as expected from the additional catechol functionality on the B ring, compared to that shown in **1**–**6** [one (for **5**); two (for **4**); three (for **1**–**3** and **6**)]. These overall interactions can position **7** in the active site gorge and sterically halt the substrate ACh binding into the catalytic triad, which could lead to its noticeable inhibitory ability against the activity of AChE.

Moving forward, **7** remarkably modified the fibrillization of metal-free Aβ and metal–Aβ and affected their corresponding preformed Aβ aggregates, as illustrated in Figs. 4, S4, and S5. In the inhibition experiments (gel/Western blots), the intensity of the bands from the sample containing **7** and metal-free $A\beta_{42}$ was reduced at *ca.* 4–20 kDa and above *ca.* 100 kDa, relative to that observed in the compound-free sample (Figs. 4b and S5a). Furthermore, smearing bands from *ca.* 20–240 kDa were noticeably detected upon incubation of Cu(II)–$A\beta_{42}$ and Zn(II)–$A\beta_{42}$ with **7**. TEM studies indicated shorter and thinner fibrils with less branching by adding **7** with metal-free $A\beta_{42}$ than those of compound-untreated metal-free $A\beta_{42}$. The morphological changes of Cu(II)–$A\beta_{42}$ and Zn(II)–$A\beta_{42}$ aggregates were also prominent upon treatment of **7**, exhibiting chopped fibrils and a mixture of amorphous and fibrillary aggregates, respectively. These reactivities of **7** were also observed in the inhibition studies with $A\beta_{40}$ (Figs. 4c and S5a) as well as the disaggregation experiments employing both $A\beta_{42}$ and $A\beta_{40}$ with and without metal ions (Figs. S4b and c and S5b).

Interaction between 7 and Aβ

Distinct reactivities of **7** towards metal-free Aβ and metal–Aβ were supported by various biophysical approaches. As displayed in Fig. S10, the chemical transformation of **7** triggered by

metal-free Aβ$_{40}$ or metal–Aβ$_{40}$ was detected by electronic absorption spectroscopy. In the absence of Aβ, an increase or decrease in the absorption of the peaks at *ca.* 265, 300, 340, and 410 nm was monitored for 24 h, which possibly resulted from the oxidation of **7**.[55] These spectral changes were accelerated upon incubation with Aβ, indicative of its impact on the oxidative modification of **7**. Such transformation of **7** was also indicated in the presence of Cu(II) or Zn(II) with and without Aβ. To probe the interaction of **7** with Aβ, their binding properties were analyzed by isothermal titration calorimetry (ITC). For the association between **7** and Aβ, we recorded the heat change upon constant titration of the compound into the solution of Aβ, where the dilution heat was also measured to avoid the heat change induced by its addition into the buffered solution. The complex of **7** and Aβ$_{42}$ or Aβ$_{40}$ was formed spontaneously and exothermically [for Aβ$_{42}$, ΔG = –6.1 (± 0.1) kcal/mol; ΔH = –0.5 (± 0.1) kcal/mol; $T\Delta S$ = 5.6 (± 0.1) kcal/mol; for Aβ$_{40}$, ΔG = –6.0 (± 0.5) kcal/mol; ΔH = –0.6 (± 0.5) kcal/mol; $T\Delta S$ = 5.4 (± 0.7) kcal/mol], which was driven by both negative enthalpy and positive entropy changes, as summarized in Figs. 6a and S11a. Binding affinities of **7** towards Aβ$_{42}$ and Aβ$_{40}$ were determined to be *ca.* 19.5 (± 0.7) and 20.5 (± 16.0) μM, respectively. Thus, **7** can interact with Aβ in a micromolar binding manner.

The amino acid residues in Aβ affected upon interaction with **7** were further investigated by two-dimensional band selective optimized flip-angle short transient-heteronuclear multiple quantum correlation nuclear magnetic resonance (2D SOFAST-HMQC NMR) spectroscopy employing both ^{15}N-labeled Aβ$_{42}$ and Aβ$_{40}$. As presented in Fig. 6b and c, the chemical shift perturbations (CSPs) provoked by adding **7** to uniformly ^{15}N-labeled Aβ$_{42}$ were detected. The Gln15, Phe19, Gly33, and Leu34 residues in Aβ$_{42}$ were changed by treatment of **7**, which implies that the compound could affect the amino acid residues adjacent to the β-turn motif (Val12–Gln15), self-recognition site (Leu17–Ala21), and *C*-terminal region (Ile32–Ala42) of Aβ$_{42}$ that are highly linked to its fibrilization.[9,56–59] Therefore, this interaction between **7** and Aβ$_{42}$ could cause a change in the conformation and aggregation propensity of Aβ$_{42}$. Moreover, the overall peak intensity of ^{15}N-labeled Aβ$_{42}$ was decreased by *ca.* 20% upon addition of **7**, suggesting the production of NMR-invisible Aβ aggregates.[60] In the case of Aβ$_{40}$, 2D SOFAST-HMQC NMR spectra obtained from ^{15}N-labeled Aβ$_{40}$ with and without **7** manifested the compound's plausible interactions with Glu3, Glu11, Phe20, and Leu34 with the reduced overall peak intensity (*ca*. 10%), as depicted Fig. S11b and c. In a similar manner to Aβ$_{42}$, **7** could alter the aggregation of Aβ$_{40}$ by interacting with the regions close to the β-turn motif (Val12–Gln15) and the self-recognition (Leu17–Ala21) and *C*-terminal (Ile32–Val40) sites that are responsible for driving amyloid formation.[9,56–59]

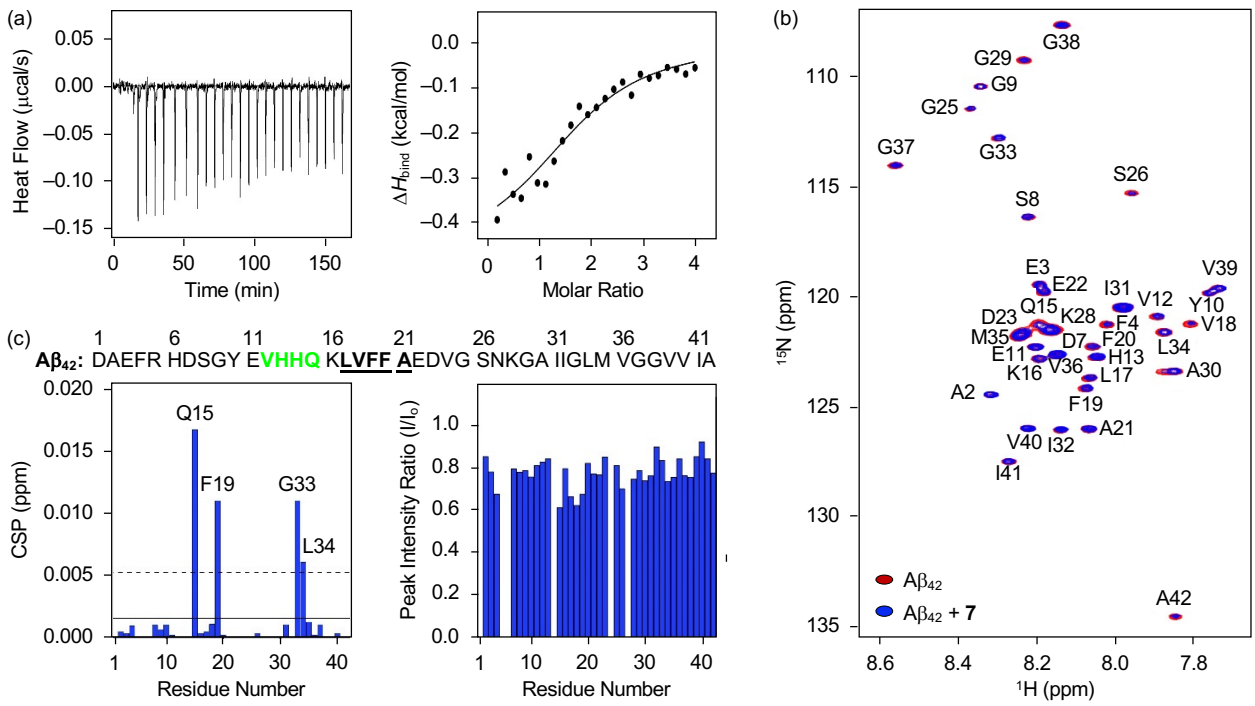

Fig. 6 Interaction of **7** with monomeric Aβ$_{42}$. (a) Binding of **7** with Aβ$_{42}$ recorded by ITC. The ITC thermogram (left) and binding isotherm (right) of **7** with Aβ$_{42}$ are depicted. The solid line indicates the best fit of the ITC data to a one-site binding model. Conditions: [Aβ$_{42}$] = 40 μM; [**7**] = 800 μM (1% v/v DMSO); 20 mM HEPES, pH 7.4; 10 °C. (b) 2D ^{1}H–^{15}N SOFAST-HMQC NMR (800 MHz) spectra of ^{15}N-labeled Aβ$_{42}$ incubated with and without **7**. (c) CSPs and peak intensity ratios of amino acid residues in ^{15}N-labeled Aβ$_{42}$ upon treatment of **7**. Amino acid residues involved in the β-turn motif and the self-recognition site are highlighted in bold (green and underline, respectively). Two horizontal lines indicate the average chemical shift (solid line) plus one standard deviation (dashed line). Conditions: [^{15}N-labeled Aβ$_{42}$] = 33 μM; [**7**] = 100 μM (1% v/v DMSO); 20 mM HEPES, pH 7.4; 10% v/v D_2O; 10 °C.

Aβ oxidation by 7

To identify the modifications of Aβ in both the absence and presence of Cu(II) upon treatment of **7**, we carried out the studies employing electrospray ionization mass spectrometry (ESI–MS). In the sample of metal-free Aβ$_{42}$ with **7**, the addition of +16 Da to the +3 charged-Aβ$_{42}$ monomer, assigned to be the oxidized monomeric Aβ$_{42}$, was detected (Fig. 7a). To determine the oxidized amino acid residues in Aβ$_{42}$, the *b* fragments generated by collision-induced dissociation were

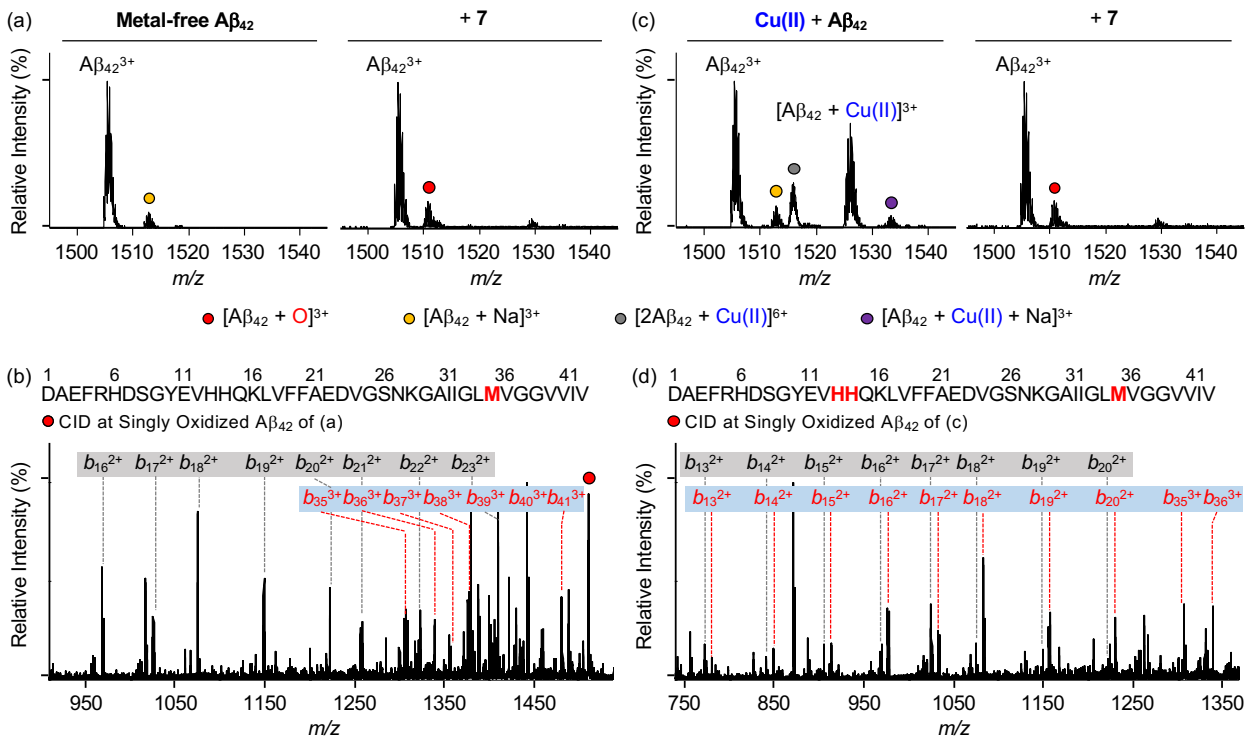

Fig. 7 Analysis of metal-free and Cu(II)-treated Aβ$_{42}$ upon addition of **7** by ESI–MS and ESI–MS^2. ESI–MS spectra of +3 charged Aβ$_{42}$ and ESI–MS^2 analyses of the singly oxidized Aβ$_{42}$ (1,511 *m*/*z*) were obtained upon incubation with **7** in the (a and b) absence and (c and d) presence of Cu(II). The peaks highlighted as a red circle correspond to the singly oxidized Aβ$_{42}$. Detailed analysis of tandem spectra is summarized in Fig. S12.† Conditions: [Aβ$_{42}$] = 100 μM; [Cu(II)] = 100 μM; [**7**] = 200 μM (1% v/v DMSO); 20 mM ammonium acetate, pH 7.4; 37 °C; 3 h; constant agitation. The samples were diluted by 10-fold with H_2O before injection into the mass spectrometer.

analyzed by tandem MS (ESI–MS^2). As illustrated in Figs. 7b and S12a, the Met35 residue was measured to be the oxidation site in the singly oxidized Aβ$_{42}$. The previous studies suggested that the His, Tyr, and Met residues in Aβ are susceptible to be oxidized and such oxidation could impact the aggregation profile of Aβ.[61–64] In particular, the oxidation of the Met residue to Met sulfoxide or sulfone can increase its polarity leading to the destabilization of β-strand structures and the decrease in hydrophobic contacts onto the *C*-terminal region that are associated with amyloid aggregation.[62,64] Similar to metal-free Aβ$_{42}$, the oxidation of Aβ$_{40}$ at the Met35 residue was monitored by incubation with **7** (Figs. S13a and b and S14a).

The oxidative modifications of Cu(II)–Aβ by addition of **7** were detected to be different from that of metal-free Aβ. As shown in Figs. 7c and S13c, the intensity of the peaks assigned to Cu(II)–$A\beta_{42}$ and Cu(II)–$A\beta_{40}$ was suppressed. When collisional energy was selectively applied to the singly oxidized Aβ produced by reacting Cu(II)–Aβ with **7**, the analysis of *b* fragments indicated the His13, His14, and Met35 residues as plausible oxidation sites, as illustrated in Figs. 7d, S12b, S13d, and S14b. In the case of His residues, their imidazole ring can involve in several intermolecular interactions, such as hydrogen bonding and π–π stacking, as the hydrogen-bond donor/acceptor and an aromatic π-motif.[65] In addition, depending on pH, both ε- and δ-nitrogen protonated His residues can mediate in the cation–π interactions with aromatic amino acid residues as well as the formation of an intramolecular salt bridge between the carboxylate group of Glu22 and the protonated His13 or His14.[65–67] Furthermore, His residues (*i.e.*, His6, His13, and His14) are included in metal coordination;[5,68] thus, the transformation of His to 2-oxo-His could disrupt intermolecular and intramolecular interactions within Aβ and its metal binding.[9,67,69] It should be noted that Cu(II) chelation by **7** can impact metal-binding properties of Aβ.[35] Therefore, oxidative modifications onto His13, His14, and Met35 by **7** could modify the aggregation of Cu(II)–Aβ. Together, our overall biophysical results and observations demonstrate the direct interactions of **7** with metal-free and metal-treated Aβ species, with the consequent modulatory effects on their aggregation.

Conclusions

To elucidate the complicate pathological nature of AD and discover effective therapeutic candidates, chemical reagents targeting and regulating multiple pathogenic components are necessary. For that purpose, this work illustrates rational strategies to develop flavonoids that can control various pathological factors found in AD-affected brains. A series of six flavonoids (**1**–**6**) was selected by adjusting the number and position of functional groups on the A ring, and their regulatory abilities against multiple pathogenic targets, including free radicals, AChE, metal-free Aβ, and metal–Aβ, were evaluated to establish the structure–activity relationship. Our investigations indicate that three hydroxyl groups on the A ring are a critical structure feature to noticeably quench free organic radicals, inhibit the activity of AChE, and modulate the aggregation of metal-free Aβ and metal–Aβ. According to the structure–activity relationships obtained from this work (for the A ring) and the previous studies (for the B and C rings),[36] we strategically fashioned the isoflavone **7** possessing three hydroxyl groups on the A ring and a catechol moiety on the B ring. Multiple reactivities of **7** against our desired targets are summarized: (i) scavenging free

organic radicals exhibiting the highest TEAC value among **1**–**7**; (ii) inhibiting the catalytic activity of AChE with a nanomolar IC_{50} value; (iii) modifying the formation of metal-free Aβ and metal–Aβ aggregates; (iv) disassembling preformed Aβ aggregates and altering their further aggregation with and without metal ions. Moreover, our computational and biophysical studies illuminate mechanistic details of **7**'s versatile reactivities towards free organic radicals, AChE, metal-free Aβ, and metal–Aβ. The relatively low redox potential and structure-based interactions with the active site gorge of AChE offer significant antioxidant and AChE inhibitory capabilities of **7**, respectively. Oxidative modifications of metal-free and metal-added Aβ through direct interactions of **7** lead to altering their aggregation profiles. Our overall studies illustrate multidisciplinary approaches for designing small molecules with multiple functions that can be used for chemical tools or therapeutic candidates in neurodegenerative disorders, such as AD.

Conflicts of interest

The authors declare no competing financial interests.

Acknowledgments

This research is supported by the National Research Foundation of Korea (NRF) grants funded by the Korean government [NRF-2022R1A3B1077319 (M.H.L.); NRF-2019R1A2C1004954 and NRF-2022R1A2C1011793 (Y.-H.L.)]; National Research Council of Science & Technology (NST) grant funded by the Korean government [CCL22061-100 (Y.-H.L.)]; KBSI fund (C220000, C230130, and C280320) (Y.-H.L.). We thank Yelim Yi for the design of the research and initial experiments and Gunhee Kim for the assistance in TEM studies.

References

1. P. H. Nguyen, A. Ramamoorthy, B. R. Sahoo, J. Zheng, P. Faller, J. E. Straub, L. Dominguez, J.-E. Shea, N. V. Dokholyan, A. De Simone, B. Ma, R. Nussinov, S. Najafi, S. T. Ngo, A. Loquet, M. Chiricotto, P. Ganguly, J. McCarty, M. S. Li, C. Hall, Y. Wang, Y. Miller, S. Melchionna, B. Habenstein, S. Timr, J. Chen, B. Hnath, B. Strodel, R. Kayed, S. Lesné, G. Wei, F. Sterpone, A. J. Doig and P. Derreumaux, *Chem. Rev.*, 2021, **121**, 2545.
2. H. J. Forman and H. Zhang, *Nat. Rev. Drug Discov.*, 2021, **20**, 689.
3. M. G. Savelieff, G. Nam, J. Kang, H. J. Lee, M. Lee and M. H. Lim, *Chem. Rev.*, 2019, **119**, 1221.
4. I. W. Hamley, *Chem. Rev.*, 2012, **112**, 5147.
5. E. Atrián-Blasco, P. Gonzalez, A. Santoro, B. Alies, P. Faller and C. Hureau, *Coord. Chem.*

Rev., 2018, **371**, 38.

6. M. P. Mattson, *Nature*, 2004, **430**, 631.
7. P. Di Mascio, G. R. Martinez, S. Miyamoto, G. E. Ronsein, M. H. G. Medeiros and J. Cadet, *Chem. Rev.*, 2019, **119**, 2043.
8. M. Mital, N. E. Wezynfeld, T. Frączyk, M. Z. Wiloch, U. E. Wawrzyniak, A. Bonna, C. Tumpach, K. J. Barnham, C. L. Haigh, W. Bal and S. C. Drew, *Angew. Chem. Int. Ed.*, 2015, **54**, 10460.
9. J. Han, Z. Du and M. H. Lim, *Acc. Chem. Res.*, 2021, **54**, 3930.
10. H. Dvir, I. Silman, M. Harel, T. L. Rosenberry and J. L. Sussman, *Chem. Biol. Interact.*, 2010, **187**, 10.
11. H. Soreq and S. Seidman, *Nat. Rev. Neurosci.*, 2001, **2**, 294.
12. Y. Zhang, J. Kua and J. A. McCammon, *J. Am. Chem. Soc.*, 2002, **124**, 10572.
13. F. J. Carvajal and N. C. Inestrosa, *Front. Mol. Neurosci.*, 2011, **4**, 19.
14. N. C. Inestrosa, J. P. Sagal and M. Colombres, *Subcell. Biochem.*, 2005, **38**, 299.
15. S. J. C. Lee, E. Nam, H. J. Lee, M. G. Savelieff and M. H. Lim, *Chem. Soc. Rev.*, 2017, **46**, 310.
16. S. Vivekanandan, J. R. Brender, S. Y. Lee and A. Ramamoorthy, *Biochem. Biophys. Res. Commun.*, 2011, **411**, 312.
17. P. Faller, C. Hureau and O. Berthoumieu, *Inorg. Chem.*, 2013, **52**, 12193.
18. J. T. Pedersen, J. Østergaard, N. Rozlosnik, B. Gammelgaard and N. H. H. Heegaard, *J. Biol. Chem.*, 2011, **286**, 26952.
19. K. P. Kepp, *Chem. Rev.*, 2012, **112**, 5193.
20. C. Cheignon, M. Tomas, D. Bonnefont-Rousselot, P. Faller, C. Hureau and F. Collin, *Redox Biol.*, 2018, **14**, 450.
21. A. I. Bush, *Trends Neurosci.*, 2003, **26**, 207.
22. P. Mecocci and M. C. Polidori, *Biochim. Biophys. Acta Mol. Basis Dis.*, 2012, **1822**, 631.
23. T. Persson, B. O. Popescu and A. Cedazo-Minguez, *Oxid. Med. Cell. Longevity*, 2014, **2014**, 427318.
24. J. W. Arndt, F. Qian, B. A. Smith, C. Quan, K. P. Kilambi, M. W. Bush, T. Walz, R. B. Pepinsky, T. Bussière, S. Hamann, T. O. Cameron and P. H. Weinreb, *Sci. Rep.*, 2018, **8**, 6412.
25. J. Sevigny, P. Chiao, T. Bussière, P. H. Weinreb, L. Williams, M. Maier, R. Dunstan, S. Salloway, T. Chen, Y. Ling, J. O'Gorman, F. Qian, M. Arastu, M. Li, S. Chollate, M. S. Brennan, O. Quintero-Monzon, R. H. Scannevin, H. M. Arnold, T. Engber, K. Rhodes, J. Ferrero, Y. Hang, A. Mikulskis, J. Grimm, C. Hock, R. M. Nitsch and A. Sandrock, *Nature*, 2016, **537**, 50.
26. K. Servick, *Science*, 2021, 372, 1141.

27. S. Kilani-Jaziri, N. Mustapha, I. Mokdad-Bzeouich, D. El Gueder, K. Ghedira and L. Ghedira-Chekir, *Tumor Biol.*, 2016, **37**, 6571.
28. N. Mateeva, S. V. K. Eyunni, K. K. Redda, U. Ononuju, T. D. Hansberry, C. Aikens and A. Nag, *Bioorg. Med. Chem. Lett.*, 2017, **27**, 2350.
29. M. Abotaleb, S. M. Samuel, E. Varghese, S. Varghese, P. Kubatka, A. Liskova and D. Büsselberg, *Cancers*, 2019, **11**, 28.
30. T. P. Cushnie and A. J. Lamb, *Int. J. Antimicrob. Agents*, 2005, **26**, 343.
31. C. A. Rice-Evans, N. J. Miller and G. Paganga, *Free Radic. Biol. Med.*, 1996, **20**, 933.
32. S. Sinha, D. H. J. Lopes and G. Bitan, *ACS Chem. Neurosci.*, 2012, **3**, 473.
33. A. Tiiman, J. Jarvet, A. Gräslund and V. Vukojević, *Biochemistry*, 2015, **54**, 7203.
34. L. N. Zhao, Y. Mu and L. Y. Chew, *Phys. Chem. Chem. Phys.*, 2013, **15**, 14098.
35. S. Park, Y. Yi and M. H. Lim, *Bull. Korean Chem. Soc.*, 2021, **42**, 17.
36. G. Nam, M. Hong, J. Lee, H. J. Lee, Y. Ji, J. Kang, M.-H. Baik and M. H. Lim, *Chem. Sci.*, 2020, **11**, 10243.
37. E. Bendary, R. R. Francis, H. M. G. Ali, M. I. Sarwat and S. El Hady, *Ann. Agric. Sci.*, 2013, **58**, 173.
38. H. J. Lee, R. A. Kerr, K. J. Korshavn, J. Lee, J. Kang, A. Ramamoorthy, B. T. Ruotolo and M. H. Lim, *Inorg. Chem. Front.*, 2016, **3**, 381.
39. Y. Xie, W. Yang, X. Chen and J. Xiao, *Food Funct.*, 2014, **5**, 2582.
40. E. Marzec, M. Świtalska, M. Winiewska-Szajewska, J. Wójcik, J. Wietrzyk, A. M. Maciejewska, J. Poznański and A. Mieczkowski, *IUBMB Life*, 2020, **72**, 1250.
41. H. Gao and J. Kawabata, *Bioorg. Med. Chem.*, 2005, **13**, 1661.
42. J. S. Derrick, R. A. Kerr, Y. Nam, S. B. Oh, H. J. Lee, K. G. Earnest, N. Suh, K. L. Peck, M. Ozbil, K. J. Korshavn, A. Ramamoorthy, R. Prabhakar, E. J. Merino, J. Shearer, J.-Y. Lee, B. T. Ruotolo and M. H. Lim, *J. Am. Chem. Soc.*, 2015, **137**, 14785.
43. M. W. Beck, J. S. Derrick, R. A. Kerr, S. B. Oh, W. J. Cho, S. J. C. Lee, Y. Ji, J. Han, Z. A. Tehrani, N. Suh, S. Kim, S. D. Larsen, K. S. Kim, J.-Y. Lee, B. T. Ruotolo and M. H. Lim, *Nat. Commun.*, 2016, **7**, 13115.
44. M. Kim, J. Kang, M. Lee, J. Han, G. Nam, E. Tak, M. S. Kim, H. J. Lee, E. Nam, J. Park, S. J. Oh, J.-Y. Lee, J.-Y. Lee, M.-H. Baik and M. H. Lim, *J. Am. Chem. Soc.*, 2020, **142**, 8183.
45. M. Kim and M. H. Lim, *Bull. Korean Chem. Soc.*, 2021, **42**, 1272.
46. N. S. Jha, S. Mishra, S. K. Jha and A. Surolia, *Electrochim. Acta*, 2015, **151**, 574.
47. M.-H. Baik and R. A. Friesner, *J. Phys. Chem. A*, 2002, **106**, 7407.
48. V. J. Forrest, Y. H. Kang, D. E. McClain, D. H. Robinson and N. Ramakrishnan, *Free Radic.*

Biol. Med., 1994, **16**, 675.
49. P. Pedrielli, G. F. Pedulli and L. H. Skibsted, *J. Agric. Food Chem.*, 2001, **49**, 3034.
50. Y. Bourne, J. Grassi, P. E. Bougis and P. Marchot, *J. Biol. Chem.*, 1999, **274**, 30370.
51. D. Grisaru, M. Sternfeld, A. Eldor, D. Glick and H. Soreq, *Eur. J. Biochem.*, 1999, **264**, 672.
52. K. Wähälä and T. A. Hase, *J. Chem. Soc., Perkin Trans. 1*, 1991, 3005.
53. Z. Sang, X. Qiang, Y. Li, W. Yuan, Q. Liu, Y. Shi, W. Ang, Y. Luo, Z. Tan and Y. Deng, *Eur. J. Med. Chem.*, 2015, **94**, 348.
54. G. Nam, Y. Ji, H. J. Lee, J. Kang, Y. Yi, M. Kim, Y. Lin, Y.-H. Lee and M. H. Lim, *ACS Chem. Neurosci.*, 2019, **10**, 3386.
55. M. Sato, K. Murakami, M. Uno, Y. Nakagawa, S. Katayama, K. Akagi, Y. Masuda, K. Takegoshi and K. Irie, *J. Biol. Chem.*, 2013, **288**, 23212.
56. J. R. Brender, A. Ghosh, S. A. Kotler, J. Krishnamoorthy, S. Bera, V. Morris, T. B. Sil, K. Garai, B. Reif, A. Bhunia and A. Ramamoorthy, *Chem. Commun.*, 2019, **55**, 4483.
57. Y. Xiao, B. Ma, D. McElheny, S. Parthasarathy, F. Long, M. Hoshi, R. Nussinov and Y. Ishii, *Nat. Struct. Mol. Biol.*, 2015, **22**, 499.
58. F. Hsu, G. Park and Z. Guo, *ACS Omega*, 2018, **3**, 8401.
59. D. Huang, M. I. Zimmerman, P. K. Martin, A. J. Nix, T. L. Rosenberry and A. K. Paravastu, *J. Mol. Biol.*, 2015, **427**, 2319.
60. K. J. Korshavn, A. Bhunia, M. H. Lim and A. Ramamoorthy, *Chem. Commun.*, 2016, **52**, 882.
61. V. N. Uversky, G. Yamin, P. O. Souillac, J. Goers, C. B. Glaser and A. L. Fink, *FEBS Lett.*, 2002, **517**, 239.
62. L. Hou, H. Shao, Y. Zhang, H. Li, N. K. Menon, E. B. Neuhaus, J. M. Brewer, I.-J. L. Byeon, D. G. Ray, M. P. Vitek, T. Iwashita, R. A. Makula, A. B. Przybyla and M. G. Zagorski, *J. Am. Chem. Soc.*, 2004, **126**, 1992.
63. A. A. Watson, D. P. Fairlie and D. J. Craik, *Biochemistry*, 1998, **37**, 12700.
64. M. Brown, J. A. Lemkul, N. Schaum and D. R. Bevan, *Arch. Biochem. Biophys.*, 2014, **545**, 44.
65. S.-M. Liao, Q.-S. Du, J.-Z. Meng, Z.-W. Pang and R.-B. Huang, *Chem. Cent. J.*, 2013, **7**, 44.
66. J. P. Lee, E. R. Stimson, J. R. Ghilardi, P. W. Mantyh, Y.-A. Lu, A. M. Felix, W. Llanos, A. Behbin, M. Cummings, M. Van Criekinge, W. Timms and J. E. Maggio, *Biochemistry*, 1995, **34**, 5191.
67. J.-M. Suh, G. Kim, J. Kang and M. H. Lim, *Inorg. Chem.*, 2019, **58**, 8.
68. P. Faller and C. Hureau, *Dalton Trans.*, 2009, 1080.
69. C. Cheignon, P. Faller, D. Testemale, C. Hureau and F. Collin, *Metallomics*, 2016, **8**, 1081.